Cornering with driving torque: steady state cornering, donuts, drifting

Illés Vörös¹, Dénes Takács^{2,3}, and Gábor Orosz^{1,4}

 Department of Mechanical Engineering, University of Michigan, Ann Arbor, MI 48109, USA, illesvoe@umich.edu, orosz@umich.edu,
 Department of Applied Mechanics, Budapest University of Technology and Economics, H-1111, Hungary, takacs@mm.bme.hu,
 HUN-REN-BME Dynamics of Machines Research Group,

Budapest, H-1111, Hungary,

⁴ Department of Civil and Environmental Engineering, University of Michigan, Ann Arbor, MI 48109, USA

Abstract. A single-track vehicle model with a variation of the brush tire model is presented that takes into account how the driving torque limits the available lateral friction of the tires. This allows us to investigate the effects of the driving torque on the different steady state maneuvers of the vehicle, which is not captured by simpler vehicle models. In addition, the vehicle model is used to design a linear feedback controller that can both initiate and stabilize drifting.

Keywords: vehicle dynamics, drifting, tire models

1 Introduction

Recent advances in vehicle automation have been focusing on controlling vehicle motion near the handling limits. This approach provides increased maneuverability to the vehicle, thereby increasing safety by avoiding potential accidents. A common simplification in the related vehicle models used for analysis and control design is to neglect the longitudinal dynamics of the vehicle by assuming a constant longitudinal speed [1]. This way the use of complex combined slip tire models [2, 3] can be avoided, but it also prevents the use of the driving torque as a control input, which is essential for controlling highly dynamic maneuvers, such as drifting [4–8].

This study presents a simple extension of the traditional lateral bicycle model so that the longitudinal dynamics can also be considered. Namely, while the lateral tire forces are modeled as functions of the side slip angle, the tires are assumed to be rigid in the longitudinal direction. Consequently, the longitudinal tire forces are calculated based on the driving torque on the wheels, limiting the available friction in the lateral direction.

The resulting model is used to analyze the effects of the driving torque on the steady state motions of the vehicle, including steady state cornering, drifting and donut maneuvers. The results provide important insights into the global dynamics of the vehicle at the handling limits, which can be used for the design of controllers that extend the maneuverability of the vehicle. As an illustrative example, a linear state feedback controller is designed that uses both the steering angle and the driving torque as control inputs to initiate and stabilize a drifting maneuver.

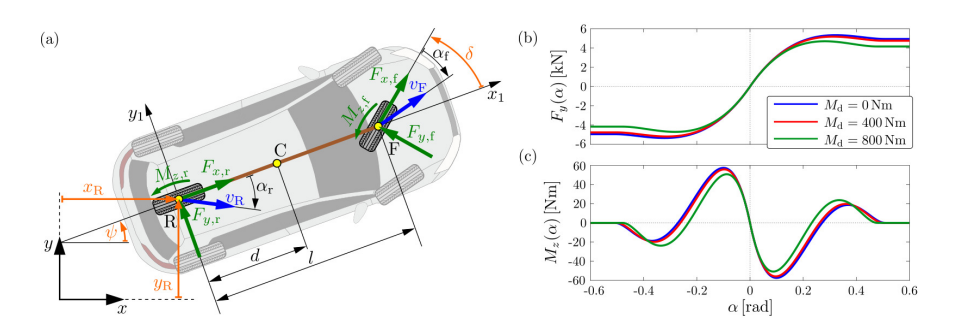


Fig. 1. Vehicle model (a), and tire side force (b) and self-aligning moment (c) characteristics for different driving torques.

2 Vehicle and tire models

This section presents the governing equations of the bicycle model (Sec. 2.1) and a modified version of the brush tire model (Sec. 2.2) that takes into account the driving torque on the wheel.

2.1 Vehicle dynamics

The analysis is based on an in-plane bicycle model (see Fig. 1(a)), where the configurational coordinates are the location of the rear axle center point (point R) $x_{\rm R}$, $y_{\rm R}$ and the yaw angle ψ . Additionally, the velocity states are defined as the longitudinal and lateral speeds of point R (u and v, respectively) and the yaw rate ω . The control inputs are the steering angle δ and the driving torque at the rear wheels $M_{\rm d}$ (which will appear through the longitudinal tire force $F_{x,\rm r}$, see Sec. 2.2). Note that the longitudinal load transfer due to the driving torque is neglected. For the derivation of the equations of motion of the vehicle, see [9].

The governing equations of the configurational coordinates are

$$\dot{x}_{\rm R} = u\cos\psi - v\sin\psi,\tag{1}$$

$$\dot{y}_{\rm R} = u \sin \psi + v \cos \psi, \tag{2}$$

$$\dot{\psi} = \omega, \tag{3}$$

Parameter Value Vehicle wheelbase (l) $2.5~\mathrm{m}$ Distance between rear axle and center of gravity (d) 1.5 m Vehicle mass (m)1400 kg $2500~\rm kgm^2$ Yaw moment of inertia $(J_{\rm C})$ Effective wheel radius $(r_{\rm w})$ 0.3 mContact patch half-length (a) $0.1 \mathrm{m}$ $2 \cdot 10^6 \, \frac{N}{m^2}$ Tire lateral stiffness per unit length (k)Sliding friction coefficient (μ) Static friction coefficient (μ_0)

Table 1. List of vehicle and tire parameters.

while the velocity states evolve according to

$$\dot{u} = v\omega + d\omega^2 + \frac{1}{m} \left(F_{x,r} + F_{x,f} \cos \delta - F_{y,f} \sin \delta \right), \tag{4}$$

$$\dot{v} = -u\omega + \frac{1}{mJ_{\rm C}} ((J_{\rm C} - md(l - d)) (F_{y,\rm f} \cos \delta + F_{x,\rm f} \sin \delta) + + (J_{\rm C} + md^2) F_{y,\rm r} - md(M_{z,\rm f} + M_{z,\rm r})),$$
(5)

$$\dot{\omega} = \frac{1}{J_{\rm C}} \left(-dF_{y,\rm r} + (l-d)(F_{y,\rm f}\cos\delta + F_{x,\rm f}\sin\delta) + M_{z,\rm f} + M_{z,\rm r} \right). \tag{6}$$

The notations of vehicle parameters along with their numerical values used in the subsequent sections are listed in Table 1. The tire forces $F_{x,i}$, $F_{y,i}$ and self-aligning moments $M_{z,i}$ (where the index $i \in \{f, r\}$ denotes the front and rear axle, respectively) are detailed in Sec. 2.2.

2.2 Tire model

The lateral tire forces and self-aligning moments are calculated based on the nonlinear brush tire model [1] as a function of the tire slip angles:

$$\tan \alpha_{\rm r} = -\frac{v}{u}, \quad \tan (\alpha_{\rm f} - \delta) = -\frac{v + l\omega}{u}.$$
 (7)

However, the brush model is modified such that the available friction of the tire depends on the longitudinal force F_x from the driving torque $M_{\rm d}$ on the wheel. Assuming that the tire is rigid in the longitudinal direction (i.e., no longitudinal slip occurs) and the mass moment of inertia of the wheel can be neglected, the longitudinal force is calculated as

$$F_x = M_{\rm d}/r_{\rm w},\tag{8}$$

where $r_{\rm w}$ is the effective wheel radius.

Assuming a parabolic distribution along the longitudinal axis of the contact patch for both the longitudinal (F_x) and the vertical force (F_z) , integrating

the forces acting on the individual bristles along the contact patch leads to the following side force and self-aligning moment characteristics (see Fig. 1(b)-(c)):

$$F_y = \begin{cases} \phi_1 \tan \alpha + \phi_2 | \tan \alpha | \tan \alpha + \phi_3 \tan^3 \alpha & \text{if} \quad 0 \le |\alpha| \le \alpha_{\text{sl}}, \\ \sqrt{F_z^2 \mu^2 - F_x^2} \operatorname{sgn}(\alpha) & \text{if} \quad |\alpha| > \alpha_{\text{sl}}, \end{cases}$$
(9)

where

$$\phi_1 = 2a^2k, \quad \phi_2 = \frac{(2a^2k)^2 \left(\sqrt{F_z^2\mu^2 - F_x^2} - 2\sqrt{F_z^2\mu_0^2 - F_x^2}\right)}{3(F_z^2\mu_0^2 - F_x^2)}, \tag{10}$$

$$\phi_3 = \frac{(2a^2k)^3 \left(3\left(F_z^2\mu_0^2 - F_x^2\right) - 2\sqrt{F_z^2\mu^2 - F_x^2}\sqrt{F_z^2\mu_0^2 - F_x^2}\right)}{27\left(F_z^2\mu_0^2 - F_x^2\right)^2},\tag{11}$$

and

$$M_z = \begin{cases} \mu_1 \tan \alpha + \mu_2 |\tan \alpha| \tan \alpha + \mu_3 \tan^3 \alpha + \mu_4 |\tan \alpha| \tan^3 \alpha \\ & \text{if } 0 \le |\alpha| \le \alpha_{\text{sl}}, \end{cases}$$
(12)

where

$$\mu_1 = -\frac{a}{3}\phi_1, \quad \mu_2 = -a\phi_2, \quad \mu_3 = -3a\phi_3,$$
 (13)

$$\mu_4 = \frac{a(2a^2k)^4 \left(-3\sqrt{F_z^2\mu^2 - F_x^2} + 4\sqrt{F_z^2\mu_0^2 - F_x^2}\right)}{81\left(F_z^2\mu_0^2 - F_x^2\right)^2}.$$
 (14)

The parameters in the above expressions include the contact patch half-length a, the lateral tire stiffness per unit length k, the sliding friction coefficient μ and the sticking friction coefficient μ_0 . The critical slip angle where total sliding starts is

$$\alpha_{\rm sl} = \arctan\left(\frac{3\sqrt{F_z^2\mu_0^2 - F_x^2}}{2a^2k}\right).$$
 (15)

The resulting lateral force at total sliding is $F_y = \sqrt{F_z^2 \mu^2 - F_x^2}$, while the self-aligning moment is zero.

Note that since a rear-wheel drive vehicle is considered in this paper, the driving torque $M_{\rm d}$ is only applied at the rear wheel and the longitudinal force is zero at the front.

3 Analysis of steady states

In this section, the effects of the driving torque on the steady state motions of the vehicle are analyzed when assuming constant inputs. Figure 2 shows the steady

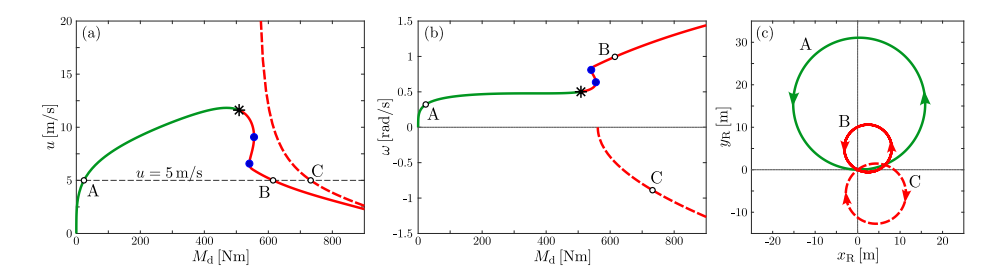


Fig. 2. Steady state solutions for steering angle $\delta = 10^{\circ}$ and increasing driving torque. (a) Longitudinal velocity, (b) yaw rate, (c) vehicle trajectories in points A, B and C.

state solutions for increasing driving torque with a steering angle of $\delta = 10^{\circ}$. Panel (a) shows the longitudinal velocity and panel (b) depicts the yaw rate of the vehicle in the steady states. The branches of steady state solutions were determined using numerical continuation with DDE-Biftool [10].

The initial stable solution for lower torque values (shown in green) corresponds to steady state cornering, characterized by a low yaw rate and increasing longitudinal velocity as the driving torque is increased. At $M_{\rm d}=507.1\,{\rm Nm}$, the steady state loses its stability through a Hopf-bifurcation (black star), and after two fold bifurcation points (blue points), the steady state turns into a donut maneuver. This unstable steady state is characterized by lower longitudinal velocity and higher yaw rate, while the vehicle is turning in the same direction as the steering angle. For sufficiently large driving torques, an additional branch of unstable steady states appears (red dashed lines). This corresponds to a drifting maneuver, where the vehicle is turning with a high yaw rate in the opposite direction from the steering angle.

The trajectory of point R of the vehicle in are plotted in Fig. 2(c) for the three steady states at the longitudinal speed $u=5\,\mathrm{m/s}$ (see the horizontal dashed line in Fig. 2(a)). It can be seen that the radius of curvature is significantly larger in steady state cornering (point A), while the donut (point B) and drifting (point C) solutions correspond to smaller turning radii. Note that in the latter case, the vehicle is turning in the opposite direction, despite the same, positive steering angle.

4 Stabilization of drifting solution

In this section, we demonstrate how a simple linear feedback controller can be designed based on the derived vehicle model to stabilize the drifting solution of the vehicle.

Let us denote the steady state drifting solution as

$$\mathbf{x}^* = \begin{bmatrix} u^* \ v^* \ \omega^* \end{bmatrix}^\mathsf{T},\tag{16}$$

corresponding to the steady state input values

$$\mathbf{u}^* = \begin{bmatrix} \delta^* \ M_{\mathrm{d}}^* \end{bmatrix}^\mathsf{T}. \tag{17}$$

The linearized system around the steady state is of the form $\dot{\tilde{\mathbf{x}}} = \mathbf{A}\tilde{\mathbf{x}} + \mathbf{B}\tilde{\mathbf{u}}$, where $\tilde{\mathbf{x}} = \mathbf{x} - \mathbf{x}^*$ and $\tilde{\mathbf{u}} = \mathbf{u} - \mathbf{u}^*$ are the state and input perturbations, respectively. Note that since the brush tire model is piece-wise smooth (see (9) and (12)), the state and input matrices \mathbf{A} and \mathbf{B} of the linearized system depend on whether the tire slip angles exceed the critical value (15) in steady state.

To design a feedback controller to stabilize drifting, we use the infinite-horizon linear quadratic regulator (LQR) approach, which solves the optimization problem

$$\min_{\tilde{\mathbf{u}}} \int_{0}^{\infty} (\tilde{\mathbf{x}}^{\mathsf{T}} \mathbf{Q} \tilde{\mathbf{x}} + \tilde{\mathbf{u}}^{\mathsf{T}} \mathbf{R} \tilde{\mathbf{u}}) \, \mathrm{d}t,
\text{s.t.} \quad \dot{\tilde{\mathbf{x}}} = \mathbf{A} \tilde{\mathbf{x}} + \mathbf{B} \tilde{\mathbf{u}}.$$
(18)

For the sake of simplicity, the state and input weight matrices are chosen to be

$$\mathbf{Q} = \begin{bmatrix} 1 & 0 & 0 \\ 0 & 1 & 0 \\ 0 & 0 & 1 \end{bmatrix}, \quad \mathbf{R} = \begin{bmatrix} 1/2 & 0 \\ 0 & 1/2 \end{bmatrix}. \tag{19}$$

The analytical solution of the optimization problem (18) yields the feedback law $\tilde{\mathbf{u}} = -\mathbf{K}\tilde{\mathbf{x}}$, where $\mathbf{K} = \mathbf{R}^{-1}\mathbf{B}^{\mathsf{T}}\mathbf{P}$ and the positive definite matrix \mathbf{P} is the solution of the algebraic Riccati equation

$$\mathbf{A}^{\mathsf{T}}\mathbf{P} + \mathbf{P}\mathbf{A} - \mathbf{P}\mathbf{B}\mathbf{R}^{-1}\mathbf{B}^{\mathsf{T}}\mathbf{P} + \mathbf{Q} = \mathbf{0}. \tag{20}$$

The overall control input to stabilize drifting is

$$\mathbf{u} = \mathbf{u}^* - \mathbf{K} \left(\mathbf{x} - \mathbf{x}^* \right), \tag{21}$$

where the gain matrix K takes the form

$$\mathbf{K} = \begin{bmatrix} 1.8844 - 0.9664 & 1.8427 \\ 0.0237 & 0.0119 & -0.0054 \end{bmatrix}$$
 (22)

for the vehicle parameters in Table 1 and the drifting solution C in Fig. 2.

Figure 3 shows a numerical simulation of how the control law (21) initiates drifting from standstill and then stabilizes it with no steady state error. Panel (a) shows the trajectory of the rear axle center point, panels (b)-(d) show the evolution of the vehicle states and panels (e)-(f) show the input signals.

It can be seen that the controller initially steers the vehicle to the left, then applies a sharp right turn to initiate drifting to the right (i.e., a turn with a negative yaw rate). Once the vehicle is sliding, the steering angle is turned back to the left to its steady state value of 10° . Note that a saturation of $\pm 30^{\circ}$ was applied to the steering angle to keep it in a realistic range.

Based on Fig. 3(f), the controller does not vary the driving torque significantly, it stays close to its steady state value even during the transients. This lesser reliance on the driving torque compared to the steering angle is also indicated by the smaller gain values in the second row of \mathbf{K} in (22).

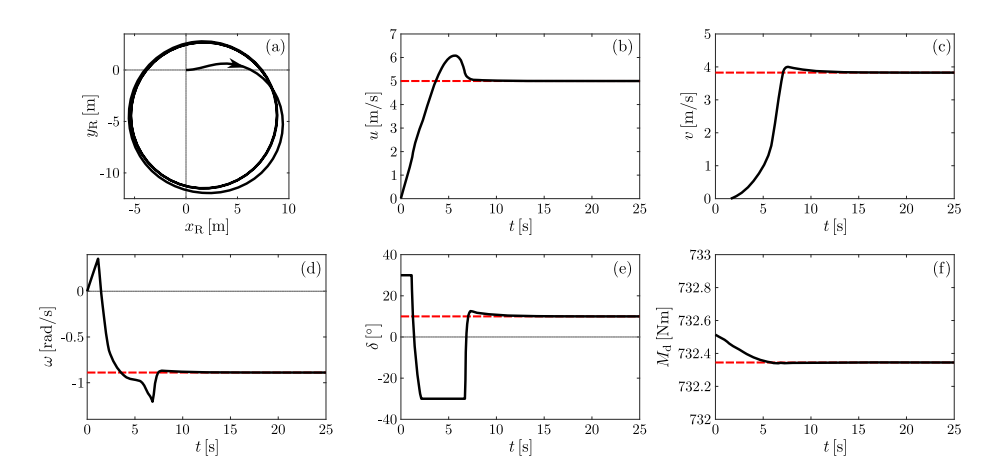


Fig. 3. Numerical simulation of stabilizing the drifting solution C in Fig. 2. (a) Trajectory of point R, (b) longitudinal velocity, (c) lateral velocity, (d) yaw rate, (e) steering angle, (f) driving torque. Dashed red lines indicate the steady state input and state values.

5 Conclusion

An extension of the classical bicycle model was presented that takes into account how the driving torque limits the available lateral friction of the tires. This allows to investigate the different steady state maneuvers of the vehicle and how they depend on the driving torque, which is not captured by simpler vehicle models. Furthermore, this extended model simplifies the design of controllers where both the steering angle and the driving torque is used as control input, without having to rely on complex combined slip tire models. This is illustrated with the design of a linear feedback controller which can both initiate and stabilize drifting.

Acknowledgments: This research is supported by the National Research, Development and Innovation Office of Hungary [grant no. NKFI-146201]. D.T. is supported by the János Bolyai Research Scholarship of the Hungarian Academy of Sciences.

References

- 1. Vörös, I., Orosz, G., Takács, D.: On the global dynamics of path-following control of automated passenger vehicles. Nonlin. Dyn. 111(9), 8235-8252 (2023). doi:10.1007/s11071-023-08284-2
- 2. Zhuang, Y., Song, Z., Gao, X., Yang, X., Liu, W.: A combined-slip physical tire model based on the vector distribution considering tire anisotropic stiffness. Nonlin. Dyn. 108(4), 2961–2976 (2022). doi:10.1007/s11071-022-07462-y
- 3. Abdulrahim, M.: On the dynamics of automobile drifting. SAE Technical Paper (2006). doi:10.4271/2006-01-1019

- 4. Goh, J.Y., Goel, T., Gerdes, J.C.: Toward automated vehicle control beyond the stability limits: drifting along a general path. J. Dyn. Sys., Meas., and Contr., 142(2), 021004 (2020). doi:10.1115/1.4045320
- Hu, C., Zhou, X., Duo, R., Xiong, H., Qi, Y., Zhang, Z., Xie, L.: Combined fast control of drifting state and trajectory tracking for autonomous vehicles based on MPC controller. In: International Conference on Robotics and Automation (ICRA), pp. 1373–1379, IEEE (2022). doi:10.1109/ICRA46639.2022.9812185
- Yang, B., Lu, Y., Yang, X., Mo, Y.: A hierarchical control framework for drift maneuvering of autonomous vehicles. In: International Conference on Robotics and Automation (ICRA), pp. 1387–1393, IEEE (2022). doi:10.1109/ICRA46639.2022. 9812110
- Peterson, M.T., Goel, T., Gerdes, J.C.: Exploiting linear structure for precision control of highly nonlinear vehicle dynamics. IEEE Trans. on Int. Veh. 8(2), 1852– 1862 (2022). doi:10.1109/TIV.2022.3171734
- 8. Edelmann, J., Eberhart, M., Steindl, A., Plöchl, M.: Post-critical behaviour of the powerslide motion. Veh. Sys. Dyn. 1–13 (2025). doi:10.1080/00423114.2025.2471346
- 9. Zhang, Y., Takács, D., Orosz, G.: From donuts to drifting and beyond: controlling the nonlinear dynamics of automated vehicles. Veh. Sys. Dyn. 1–36 (2025). doi: 10.1080/00423114.2025.2522391
- Engelborghs, K., Luzyanina, T., Roose, D.: Numerical bifurcation analysis of delay differential equations using DDE-BIFTOOL. ACM Trans. on Math. Soft. 28(1), 1– 21 (2002). doi:10.1145/513001.513002